to this IUCF annual report.

2) P. Schwandt, IUCF Report No. 7-79 (unpublished).

3) E.H. Auerbach, Computer Physics Communications 15, 165 (1978).

4) H.M. Pilkuhn, Relativistic Particle Physics, Springer, New York, 1979.

5) L. Ray et al., Phys. Rev. C18, 2641 (1978).

6) J.R. Comfort and B.C. Karp, Phys. Rev. C21, 2162 (1980).

7) M.L. Goldberger and K.M. Watson, Collision Theory, Krieger, New York, 1975.

8) M. Jaminon, C. Mahaux, and P. Rochus, Phys. Rev. C22, 2027 (1980).

ENERGY-DEPENDENT FORM FACTORS OF THE OPTICAL POTENTIAL FOR INTERMEDIATE-ENERGY PROTONS FROM A RELATIVISTIC MODEL

P. Schwandt
Indiana University Cyclotron Facility, Bloomington, Indiana 47405

L.G. Arnold and B.C. Clark
The Ohio State University, Columbus, Ohio 43210

R.L. Mercer
Watson Research Center, IBM Corp., Yorktown Heights, New York 10598

Realistic Brueckner-Hartree-Fock (BHF) calculations[1,2,3] of the optical potential in nuclear matter lead to very different energy-dependences of the real potential strength for different values of the matter density. When applied to finite nuclei in a local density approximation (LDA), this results in potential radial shapes which in the 150-400 MeV "transition" region of nucleon kinetic energy differ drastically from the radial shape of the nuclear matter density distribution. Specifically, in the (normal-density) interior of the nucleus the potential changes from attractive to repulsive at a much lower energy (200-250 MeV) than in the (low-density) nuclear surface where the potential remains weakly attractive even at several hundred MeV. A characteristic "wine-bottle-bottom" shape for the real central potential in the transition energy region is thus a natural result of the BHF approximation.

Strikingly similar energy-dependent potential shapes are obtained in an entirely different approach to the microscopic formulation of the optical potential, namely the relativistic Dirac-equation model (or Dirac-Hartree model) based on essentially static, heavy-meson exchange nucleon-nucleon (NN) interactions[4,5]. The relativistic treatment of the many-body system in its simplest form leads to an average, local one-body potential which is the sum of a Lorentz scalar field, U_s, and the 4th (time-like) component, U_o, of a Lorentz vector field. The Dirac equation for the one-body wavefunction with these potentials is written as ($\hbar = c = 1$):

$$\{\vec{\alpha}\cdot\vec{p} + \beta[m + U_s(r)] + [U_o(r) + V_c(r)]\}\psi_D(\vec{r}) = E\psi_D(\vec{r})$$

where $V_c(r)$ is the Coulomb field, m the nucleon mass and E the nucleon total energy in the c.m. frame. For positive-energy (scattering) states the Dirac equation potentials U_s, U_o are taken to be complex:

$$U_s(r) = V_s f_s(r) + iW_s g_s(r),$$
$$U_o(r) = V_o f_o(r) + iW_o g_o(r).$$

One expects V_s to be attractive since its origin is in neutral scaler meson exchange, and V_o to be repulsive since it is associated with the exchange of neutral vector mesons. The form factors $f_s(r)$ and $f_o(r)$ for the real parts of U_s and U_o are identified with effective scalar and vector target density distribu-

tions related to the shape of the target nucleus, corrected for finite nucleon size and finite range of the respective scalar and vector meson- exchange NN forces.

To make contact with results of optical-model analyses based on the conventional nonrelativistic Schrödinger equation, one may perform a standard reduction of the Dirac equation to second-order form for the large (upper) component, ψ_u, of the Dirac spinor ψ_D. One then obtains a Schrödinger-like equation with an explicitly momentum-and energy-dependent effective potential:

$$[p^2 + 2E(U_c + U_{so}\,\vec{\sigma}\cdot\vec{L})]\,\psi_u(\vec{r}) = [(E - V_c)^2 - m^2]\,\psi_u(\vec{r})$$

where

$$U_c = \frac{1}{2E}[2EU_o + 2mU_s - U_o^2 + U_s^2 - 2V_cU_o + iU_D\vec{r}\cdot\vec{p}]$$

$$U_{so} = -U_D = -\frac{1}{2E}\frac{1}{Br}\frac{\partial B}{\partial r}, \qquad B \equiv \frac{E+m+U_s-U_o-V_c}{E+m}\,.$$

One may identify U_c and U_{so} as effective "Schrödinger-equivalent" central and spin-orbit potentials. The particularly noteworthy and attractive general features of these Schrödinger-equivalent potentials are

--U_c, U_{so} are explicitly energy dependent even for static Dirac-equation potentials U_s, U_o. To a great extent the primary consequence of non-locality is thus taken into account.

--The spin-orbit term U_{so} arises naturally in the model and is intrinsically coupled with the central term U_c through their respective dependences on U_s, U_o.

--The real part of U_c depends on both real and imaginary parts of U_s, U_o which appear in both linear and quadratic form. This quadratic dependence on the Dirac potentials, coupled with a small difference in radial extent of the form factors $f_s(r)$ and $f_o(r)$ arising from the mass difference of the exchanged mesons, accounts for the explicit energy-dependence of the shape of $\mathrm{Re}U_c$, which is such that $\mathrm{Re}U_c$ changes sign at a lower energy in the nuclear interior than in the nuclear surface.

--The explicit appearance of the Coulomb term V_c in the expressions for the effective central and spin-orbit potentials gives rise to an intrinsic isospin dependence for these terms.

In order to illustrate the characteristic features of the effective Schrödinger-equivalent potential and to demonstrate the basic validity of the relativistic optical model, we present here some model calculations for intermediate-energy proton elastic scattering from ^{40}Ca in general and comparison with IUCF experimental data for $\vec{p} + {}^{40}$Ca at 181 MeV in particular. The basic procedure of the calculations is outlined here only briefly; a much more detailed description can be found in a forthcoming publication by the present authors.[6]

The form factors $f_s(r)$ and $f_o(r)$ of the real parts of U_o and U_s were chosen to be 2-parameter Fermi functions $[1 + \exp(r-c)/z]$ prescribed by convolution of effective target nucleon densities with simple NN interactions of Yukawa form representing exchanges of σ (scalar) and ω (vector) mesons of effective masses 550 and 780 MeV, respectively. These form factors f_s, f_o were then kept fixed while the corresponding strengths V_s, V_o were treated as free parameters in fitting the 181 MeV ^{40}Ca data, starting with initial values V_s = -470 MeV and V_o = 383 MeV given by the mean field theory of nuclear matter. The imaginary parts of U_s

Table 1. Parameters of the Lorentz scalar (U_S) and Lorentz vector (U_O) potentials determined in the Dirac-equation analysis of 181 MeV $\vec{p}$ + ^{40}Ca data. Parameters in parentheses were held fixed in the analysis. Negative strength denotes attraction.

Potential	Strength(MeV)	c(fm)	z(fm)
ReV_O	334	(3.474)	(0.668)
ImV_O	-107	3.487	0.716
ReV_S	-437	(3.453)	(0.692)
ImV_S	109	(3.453)	(0.692)

and U_O were treated phenomenologically, with initial geometry constraints $g_S(r) = f_S(r)$ and $g_O(r) = f_O(r)$. A fair representation of the elastic scattering data was obtainable by adjusting the 4 strength parameters V_S, V_O, W_S, W_O. Much better fits to angular distributions $\sigma(\theta)$, $A(\theta)$ and to the reaction cross section σ_R were obtained by allowing the 4 strength parameters and the 2 shape parameters of $g_O(r)$ to vary.

The resulting optimum parameters of the Lorentz vector and scalar potentials determined in the analysis of 181 MeV $\vec{p}$ + ^{40}Ca data are given in Table 1. (The parameters in parentheses were kept fixed in the analysis). The resulting fits to the $\vec{p}$ + ^{40}Ca angular distributions are presented in Fig. 1. The radial dependences of the effective Schrödinger-equivalent central and spin-orbit potentials in the relativistic model (ROM) are illustrated in Fig. 2. The dashed curves labelled SOM in Fig. 2 are corresponding results of a standard nonrelativistic model analysis using conventional Fermi-function (Woods-Saxon) potential form factors which yield largely equivalent fits to the data. Although the relativistic Dirac-equation model has now been shown[7] to describe proton elastic scattering over a wide energy range (20 MeV-1 GeV) and hence can be considered as a valid alternative to the standard Schrödinger-equation formulation, the relatively narrow momentum transfer range (generally $q \lesssim 3$ fm^{-1}) covered by the available data unfortunately does not permit unambiguous discrimination between these drastically different potential-model prescriptions. The need for the unorthodox potential shapes provided by the relativistic Dirac-Hartree model, or by BHF calculations in the LDA,[8] to describe elastic scattering data in the transition energy range is not yet firmly established, but some evidence for this was provided by recent high-q measurements for $\vec{p}$ + ^{12}C at 200 MeV.[9]

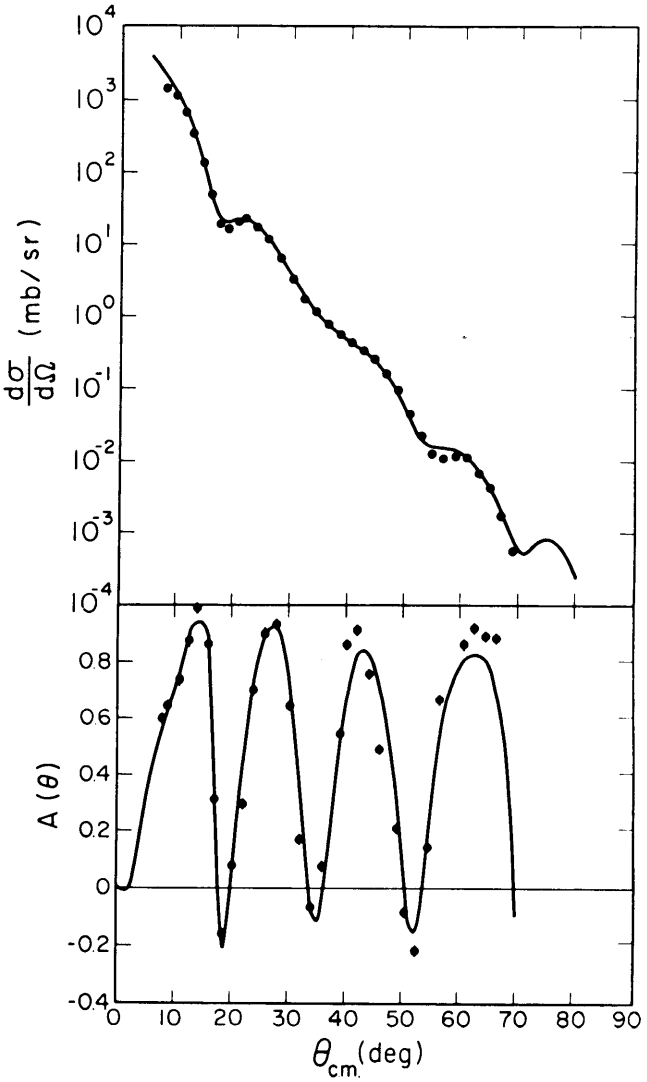

Figure 1. Elastic $\vec{p}$ + ^{40}Ca cross sections and analyzing powers at 181 MeV (IUCF data). The curves are results of the relativistic optical-model analysis described in the text.

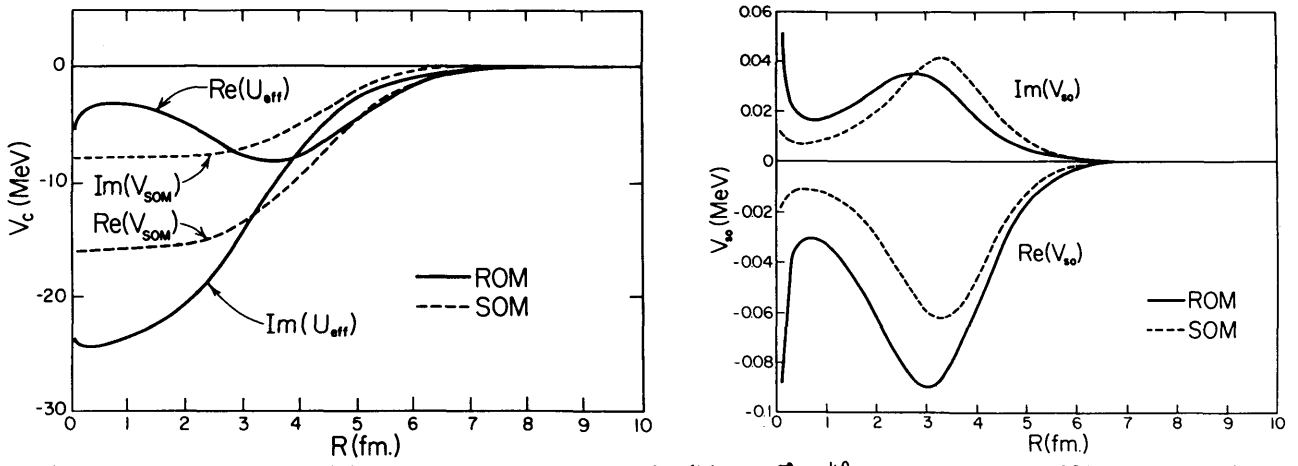

Figure 2. Central potentials (a) and spin-orbit potentials (b) for $\vec{p}$ + ^{40}Ca scattering at 181 MeV. Solid curves show the real and imaginary parts of the relativistic effective potentials (ROM), dashed curves are the corresponding results from a standard nonrelativistic analysis (SOM).

Assuming static Dirac-Hartree potentials U_S, U_O whose parametrization (for the case of ^{40}Ca, Table 1) is fixed by fitting data at one energy within the transition region, we can proceed to calculate the energy dependence of the effective Schrödinger-equivalent potentials U_C, U_{SO}. For ^{40}Ca over the energy range 50-500 MeV, the results are illustrated in Figs. 3 and 4. The real central potential, ReU_C, is seen to be attractive at all radii up to 200 MeV and has the familiar Fermi-function-like shape below 150 MeV. Above 500 MeV, ReU_C has become repulsive everywhere and in shape qualitatively follows the nuclear matter distribution, in agreement with our expectation from first-order impulse-approximation calculations of the optical potential which successfully describe proton elastic scattering at 800 MeV, for example.[10] In the transition energy region (roughly 200-500 MeV) the pronounced deviation from a monotonic potential is clearly evident; ReU_C is characterized by a repulsive interior and an attractive surface or tail region, which explains the demonstrable failure[11] of the first-order impulse approximation (IA) in this energy region.

The imaginary central potential, ImU_C, exhibits the expected monotonic Fermi-function-like shape (representative of absorption roughly proportional to the target nucleon density) and the expected rapid increase in strength with energy above 100 MeV.

The spin-orbit potential (Fig. 4) qualitatively follows the general trend with energy predicted by most microscopic models, i.e., a slow decrease in both the real and imaginary spin-orbit strength parameters, with little change in shape, and nearly constant strength ratio $ImU_{SO}/ReU_{SO} \simeq -1/3$.

These trends of the effective central and spin-orbit potentials with energy are also illustrated in a slightly different fashion in Fig. 5 where the corresponding potential volume integrals (normalized by the number of target nucleons) are displayed as a function of proton energy. The relativistic model results, shown here by the heavy dashed curves labelled DH (for Dirac-Hartree), are compared to predictions of other microscopic optical-potential models,[2,12,13] and to results of phenomenological, nonrelativistic optical-model analyses[14] of available data between 40 and 1000 MeV (using Woods-Saxon form factors for the central

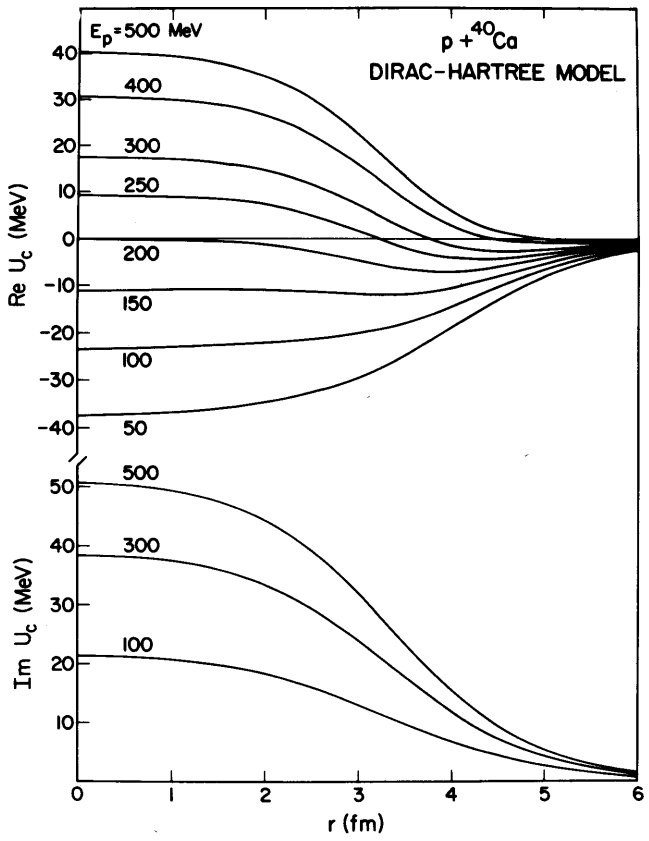

Figure 3. Radial variation of the real and imaginary parts of the relativistic effective central potential for proton energies between 100 and 500 MeV.

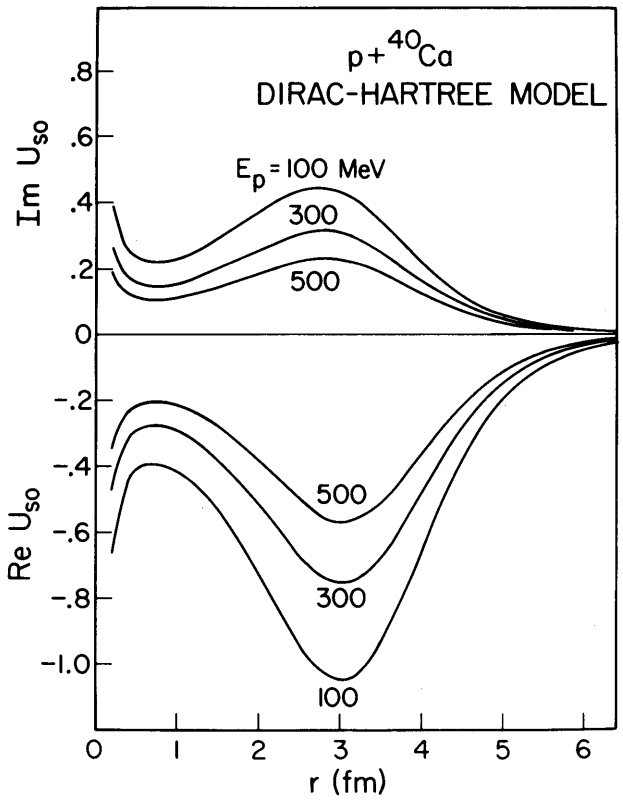

Figure 4. Radial variation of the real and imaginary parts of the relativistic effective spin-orbit potential for proton energies between 100 and 500 MeV.

potential). While the predicted energy dependence shown here for the relativistic Dirac-Hartree model is not correct in detail (fits to data at 500 and 800 MeV show the need for some mild energy dependence of the Dirac potential strength ratios V_o/V_s and W_o/W_s, which was ignored here), the overall qualitative agreement with trends of BHF results at low energies and of IA predictions at high energies is remarkable, considering the enormous energy range and the use of static (energy-independent) NN interactions as input into the Dirac-equation model. In the case of the spin-orbit potential, we suspect that the strong and non-monotonic energy dependence exhibited by the results of the phenomenological analysis in the transition energy range, in marked disagreement with both BHF and Dirac-Hartree calculations, is an artifact of the analysis procedure in which the real central potential was forced to have a Woods-Saxon shape.

In conclusion, the use of a Dirac-equation optical model is an attractive alternative to the standard nonrelativistic Schrödinger-equation approach since it not only (1) reproduces a number of characteristic macroscopic features of the effective Schrödinger-equivalent potential (which do in fact seem to be required by high-momentum-transfer experiments) and (2) clearly exhibits the fundamental connection between central and spin-orbit effective potentials and their intrinsic energy dependence, but also (3) provides the necessary phenomenological basis for the description of the nuclear many-body problem in terms of meson-exchange descriptions of the fundamental NN force.

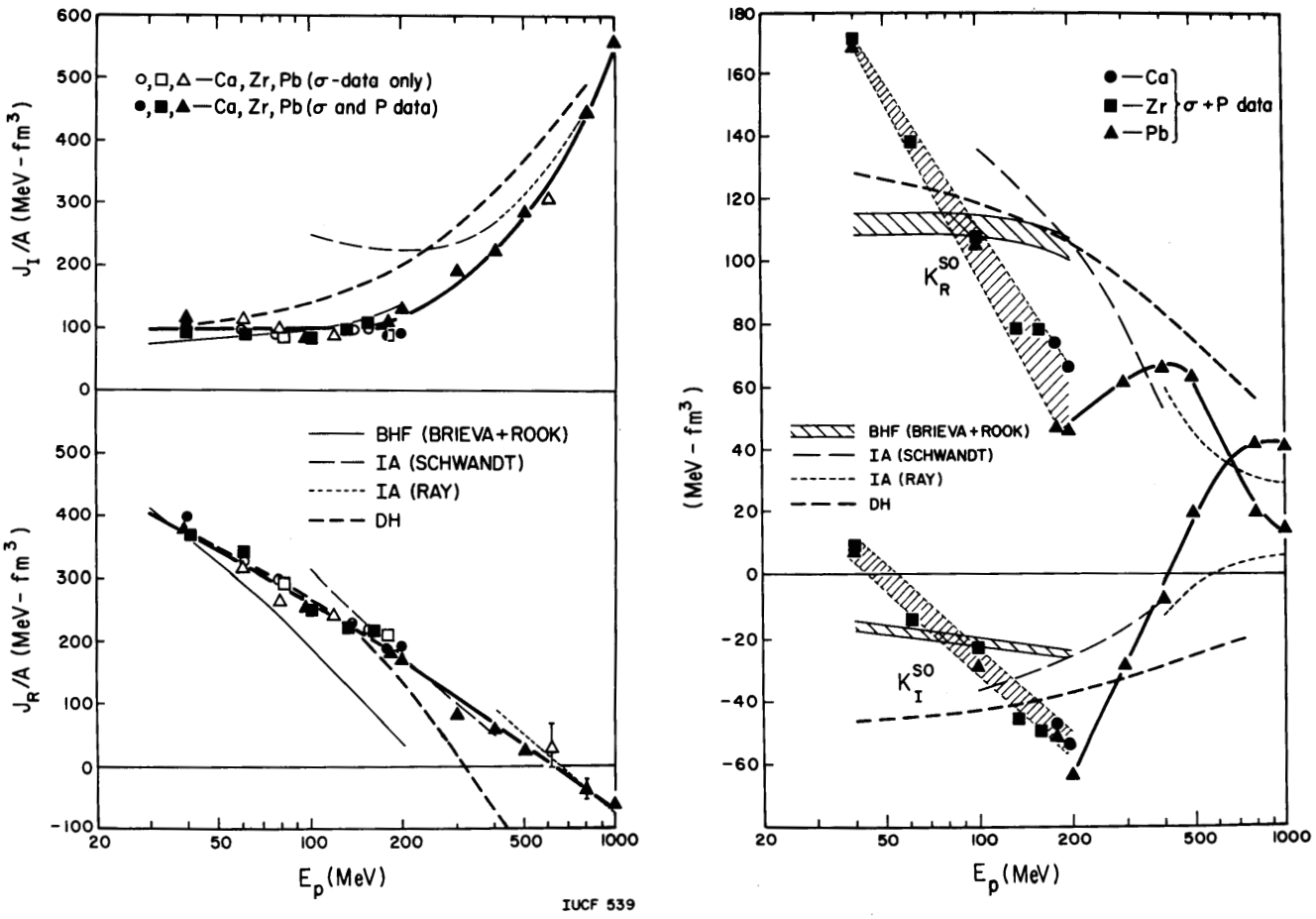

Figure 5. Normalized volume integrals of the central (a) and spin-orbit (b) optical potentials for proton scattering between 40 and 1000 MeV. The relativistic model results are shown by the heavy dashed curves labelled DH. The solid symbols represent results of nonrelativistic phenomenological (Woods-Saxon) potential fits to cross section and polarization data for the nuclei indicated on the legend; the heavy solid curves are smooth lines connecting these "data" points. The BHF results shown are from ref. 2, the impulse-approximation (IA) results from refs. 12, 13.

1) C. Mahaux, Proceed. Conf. on Microscopic Optical Potentials, Hamburg, 1978, p.1.

2) F.A. Brieva and J.R. Rook, Nucl. Phys. A291, 299 and 317 (1977).

3) V.R. Pandharipande, to be published.

4) M. Jaminon, C. Mahaux and P. Rochus, Phys. Rev. C22, 2027 (1980).

5) L.G. Arnold, B.C. Clark and R.L. Mercer, Phys. Rev. C19, 917 (1979); ibid., B.A.P.S. 25, 520 (1980).

6) L.G. Arnold, B.C. Clark, R.L. Mercer and P. Schwandt, to be published in Phys. Rev. C (in press).

7) B.C. Clark, L.G. Arnold and R.L. Mercer, B.A.P.S. 25, 741 (1980).

8) H.V. Geramb, F.A. Brieva and J.R. Rook, Proceed. Conf. on Microscopic Optical Potentials, Hamburg, 1978, p. 104.

9) H.O. Meyer, P. Schwandt, G.L. Moake and P.P. Singh, Phys. Rev. C23, 616 (1981).

10) G. Igo et al., Phys. Lett. 81B, 151 (1979) and references therein.

11) P. Schwandt, unpublished.

12) P. Schwandt, B.A.P.S. 24, 824 (1979).

13) L. Ray, Phys. Rev. C20, 1857 (1979).

14) P. Schwandt et al., Contribution 2.24, 5th Intern. Symposium on Polarization Phenomena in Nucl. Phys., Santa Fe, Aug. 11-15, 1980.